Crystals usually grow (*11*) as regular polyhedra or as dendritic structures which may have dislocations but do not have the kind of regular 3 by 3 internal structure shown in Fig. 1.

There are obviously many unanswered questions. For example, why are the small metallic particles cubes? Why is the 3 by 3 by 3 superstructure of the large particles stable? In this connection it should be noted that in experiments (*12*) in which particles are formed by spraying atoms out of a nozzle, some configurations are much more stable than others.

REFERENCES AND NOTES

1. R. Pflaum, P. Pfau, K. Sattler, E. Recknagel, *Surf. Sci.* **156**, 165 (1985).
2. G. M. Chow *et al.*, *Appl. Phys. Lett.* **56**, 1853 (1990).
3. G. M. Chow, C. L. Chien, A. S. Edelstein, *J. Mater. Res.* **6**, 8 (1991).
4. For reviews see R. Uyeda, *J. Cryst. Growth* **24/25**, 69 (1974); C. Hayashi, *J. Vac. Sci. Technol. A* **5**, 1375 (1987).
5. P. Chaudhari and J. W. Matthews, *Appl. Phys. Lett.* **17**, 115 (1970).
6. F. F. Abraham, *Homogeneous Nucleation Theory* (Academic Press, New York, 1974).
7. A preliminary investigation indicates that the unusual particle formation is less prevalent if the substrate is not cooled.
8. Such columnar growth is typical when the substrate temperature is much less than the melting temperature.
9. R. A. Buhrman and C. G. Granqvist, *J. Appl. Phys.* **47**, 2200 (1976).
10. C. Kaito, *Jpn. J. Appl. Phys.* **17**, 601 (1978).
11. H. E. Buckley, *Crystal Growth* (Wiley, New York, 1961).
12. W. D. Knight *et al.*, *Phys. Rev. Lett.* **52**, 2141 (1984).

13. The authors gratefully acknowledge the Office of Naval Research for their financial support, J. M. Cowely for a portion of the electron microscopy study, R. K. Everett and E. McCormich for assistance, J. Karle and B. B. Rath for helpful discussions, and J. Karle, B. B. Rath, A. C. Ehrlich, S. C. Sanday, and D. J. Nagel for critical reading of the manuscript. This work was done while G.M.C. and E.I.A. were, respectively, research associates of the National Research Council and the Office of Naval Technology.

1 October 1990; accepted 6 February 1991

San Andreas Fault Zone Head Waves Near Parkfield, California

YEHUDA BEN-ZION* AND PETER MALIN†

Microearthquake seismograms from the borehole seismic network on the San Andreas fault near Parkfield, California, provide three lines of evidence that first *P* arrivals are "head" waves refracted along the cross-fault material contrast. First, the travel time difference between these arrivals and secondary phases identified as direct *P* waves scales linearly with the source-receiver distance. Second, these arrivals have the emergent wave character associated in theory and practice with refracted head waves instead of the sharp first breaks associated with direct *P* arrivals. Third, the first motion polarities of the emergent arrivals are reversed from those of the direct *P* waves as predicted by the theory of fault zone head waves for slip on the San Andreas fault. The presence of fault zone head waves in local seismic network data may help account for scatter in earthquake locations and source mechanisms. The fault zone head waves indicate that the velocity contrast across the San Andreas fault near Parkfield is approximately 4 percent. Further studies of these waves may provide a way of assessing changes in the physical state of the fault system.

EMERGENT FIRST ARRIVALS IN SEISmic records of earthquake monitoring networks often confuse efforts to interpret the initial ground motion caused by an earthquake. Emergent phases have been ascribed to various wave-propagation effects in the earth, such as refraction along horizontal layer boundaries and intrinsic attenuation of an otherwise sharp direct pulse. In this report, we discuss observational evidence for emergent first arrivals resulting from vertical material boundaries at a major crustal fault. On the basis of travel time and first motion polarity differences between emergent and sharp arrivals from Parkfield area earthquakes, we propose that the emergent arrivals are fault zone head waves refracted along the material contrast between the two sides of the San Andreas fault (*1–3*).

Figure 1 shows schematic ray paths of head waves and regular geometrical arrivals for subsurface receivers in a simplified fault zone geometry consisting of two quarter-spaces. In the higher velocity medium 1, there are two arrivals. The first is the direct wave, and the second is the wave reflected by the free surface. In the lower velocity medium 2, on the other hand, there are four distinct arrivals. The first is the head wave, the second is the direct wave, the third is a head wave reflected by the free surface, and the fourth is the free surface reflection of the direct wave.

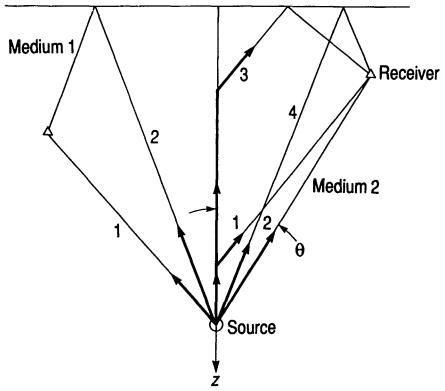

Fig. 1. Ray paths in faster (medium 1) and slower (medium 2) joined quarter-spaces; θ denotes the source-receiver angle used in Fig. 2.

The waveform character and motion polarity of head waves and direct arrivals are illustrated in Fig. 2. In the faster medium the first motion is that of a sharp direct wave, whereas in the slower medium gradual buildup of head wave amplitude produces an emergent pulse that precedes the sharp opposite polarity motion of the direct wave (*1*). In the absence of material contrast, the waves to the right of the fault are the reversed images of the sharp direct waves at corresponding points to the left of the fault.

To obtain field evidence for fault zone head waves, we examined seismograms from 75 microearthquakes in the Parkfield section of the San Andreas fault (*4*) (Fig. 3). The

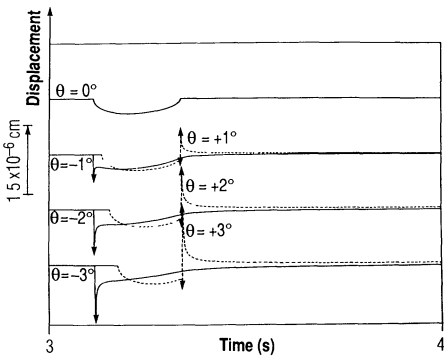

Fig. 2. Comparison of near-fault synthetic seismograms in faster (solid lines) and slower (dashed lines) joined quarter-spaces. Media velocities are 3.2 and 3.0 km/s, respectively. An antiplane line source dislocation of 1 cm operates at a depth of 10 km along the material interface at time = 0. Receivers are on the free surface at angular offset from the fault indicated by θ (positive clockwise). [Adapted from (*1*)]

Department of Geological Sciences, University of Southern California, Los Angeles, CA 90089 and Institute of Crustal Studies, University of California at Santa Barbara, CA 93106.

*Present address: Department of Earth and Planetary Sciences, Harvard University, 24 Oxford Street, Cambridge, MA 02138.
†Present address: Department of Geology, Duke University, Durham, NC 27706.

events were chosen because they occurred near the fault and gave initial evidence for fault zone head waves. The features we looked for were an emergent first motion typical of a head wave, followed by a sharp opposite polarity arrival that might represent the direct wave.

As in the seismological study of horizontal layering, the strongest evidence for a lateral material contrast comes from travel time differences between head waves and direct arrivals. This difference should increase with distance traveled along the boundary and decrease with source and receiver distance from the boundary. Another conspicuous indication of lateral material contrast, although less robust because of difficulties in the accurate determination of earthquake focal mechanisms, is that of reversed first motion polarities. To compare the sense of first motion of the potential head waves to what is expected from wave propagation theory, we assumed that the candidate earthquakes were slip events along the San Andreas fault. Precise determination of actual fault plane motions is difficult to obtain because of the lack of good station coverage. With this assumption, all first motions to the southwest of the events should be opposite those to the southeast, if there is no velocity contrast across the San Andreas fault.

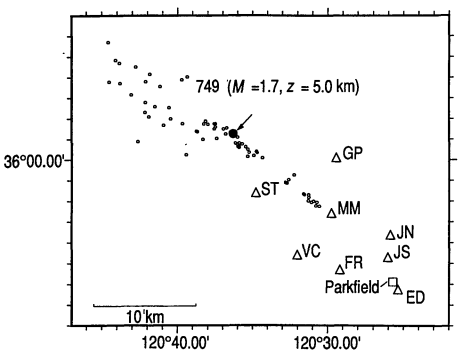

Fig. 3. Plan of the Parkfield, California, borehole seismic network. Borehole seismometers are denoted by triangles. The town of Parkfield is shown by a box. Circles indicate epicenters of 75 microearthquakes used in this study. The large solid circle marks the event used in Fig. 4 to illustrate the waveforms and first motion polarities of fault zone head waves and direct *P* arrivals. *M* and z denote moment magnitude and earthquake depth, respectively.

Theoretical analysis of head waves along a vertical interface (*1, 2*) shows that there is a critical receiver distance x_c from the interface within which the head waves are the first arrivals. The critical distance is given by

$$x_c = r \tan[\cos^{-1}(\alpha_2/\alpha_1)] \qquad (1)$$

where r is the distance the wave travels along the fault, and α_2 and α_1 are the average *P* wave velocities of the slower and faster media, respectively. The head waves will have the same polarity as corresponding direct waves in the faster medium (Fig. 2). The rock types and average *P* wave velocities near Parkfield, California, are Gabilan granite with $\alpha_G \sim 5.5$ km/s west of the fault and a slower Franciscan rock with $\alpha_F \sim 5.3$ km/s east of the fault (*5–7*). If these values are used in Eq. 1, x_c is ~2.8 km for $r = 10$ km. For station MM with a normal distance from the fault $x = 0.5$ km and station ED with $x = 1.5$ km (Fig. 3), head waves with the same polarity of the stations on the opposite side of the fault will be the first arrivals for most San Andreas fault earthquakes. For the other Franciscan block stations the situation is more varied, depending on r and the average velocity contrast.

Table 1. Parameters for head wave first arrivals during event 749; x is station offset from the fault; r is station distance from source along the fault; x_c is critical offset from the fault (see Eq. 1) for head wave first arrival. Station locations are shown in Fig. 3.

Station	x (km)	r (km)	x_c (km)
MM	0.5	11.0	3.0
ED	1.5	20.2	5.6
JS	2.5	17.4	4.8
JN	4.5	16.2	4.5
GP	5.5	9.3	2.6

Seismograms from a sample microearthquake (Fig. 4) illustrate the emergent first arrivals, sharper secondary waves, differing travel times, and reversed first motion polarities of fault zone head waves. The sample event occurred below all the major horizontal layers known at Parkfield (*7*); therefore, the emergent waves east of the San Andreas fault cannot be explained as head waves along these layers. At the three stations on the faster crustal block west of the fault (ST, VC, and FR), the first motions are sharp upward pulses. At the slower block east of the fault, stations MM, ED, and JS are within the critical distance for first arriving head waves, whereas JN is at the critical distance and GP is beyond it (Table 1). The waveform character and motion polarity observed at all stations are consistent with the

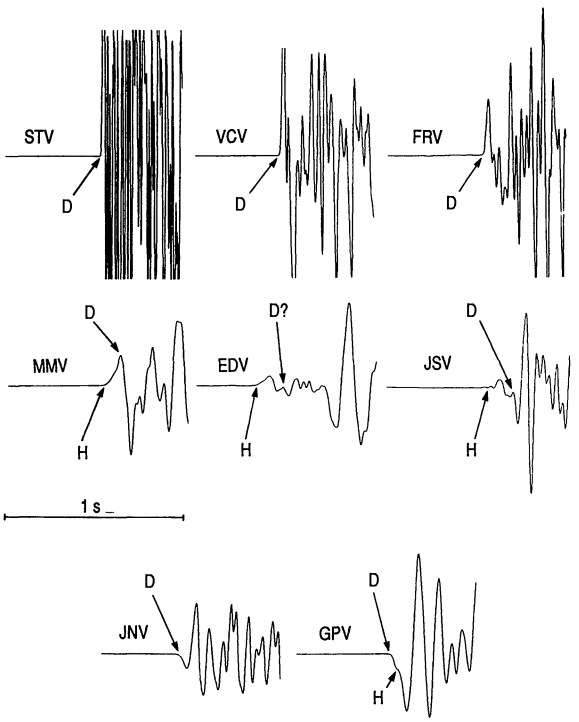

Fig. 4. One-second vertical seismograms of earthquake 749 ($M = 1.7$, $z = 5.0$ km). The top panel shows records of stations located on the faster rock west of the fault. The two lower panels show records of stations located on the slower rock east of the fault. In the lower panels, distance away from the fault increases to the right. Arrows labeled D and H point to direct and head wave arrivals, respectively. The amplitude plotting scales of the seismograms are not the same.

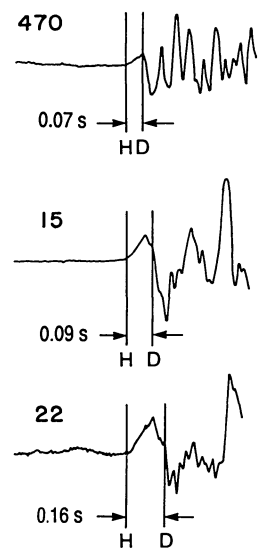

Fig. 5. A series of 1-s vertical seismograms at MM showing head and direct arrival time picks for earthquakes 470 ($r \sim 10$ km), 15 ($r \sim 16$ km), and 22 ($r \sim 25$ km).

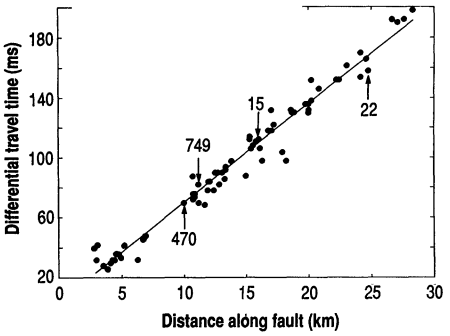

Fig. 6. Time difference between direct and head wave arrivals at MM during the 75 microearthquakes of Fig. 3 plotted against the distance the waves travel along the fault. The events of Figs. 4 and 5 are indicated by arrows. The line shows a least-squares fit of Eq. 2 through the data, indicating a roughly 4% average material contrast across the San Andreas fault at Parkfield.

head wave interpretation. At station GP an up step of a secondary head wave follows the down motion of the direct arrival.

The time difference between fault zone head waves and direct arrivals is approximately

$$\Delta t \sim r[(1/\alpha_2) - (1/\alpha_1)] \sim r(\Delta\alpha/\alpha^2) \quad (2)$$

so that the time separation between the head waves and direct arrivals scales with the distance traveled along the fault. If the arrivals can be correctly identified and timed, the slope $[\Delta t(r_2) - \Delta t(r_1)]/(r_2 - r_1)$ of their time difference versus distance can be used to estimate the average velocity contrast across the fault.

Figure 5 illustrates the data used to examine the time-distance scaling of fault zone head waves and direct arrivals. In the top trace ($r \sim 10$ km) the head wave is a short emergent pulse, truncated by the closely following sharper direct P wave with initial motion of opposite polarity. As the distance from the source increases, the head wave broadens considerably, whereas the direct wave continues to be a relatively sharp, opposite-polarity arrival. The time difference against distance for such first arriving head waves and secondary direct waves for our data (Fig. 6) has a slope

$$s \sim \Delta\alpha/\alpha^2 \sim 0.007 \text{ s/km} \quad (3)$$

For $\alpha = 5.5$ km/s in Eq. 3, the velocity contrast, $\Delta\alpha/\alpha$, across the San Andreas fault near Parkfield is approximately 4%. This value is similar to the contrast used to calculate the expected critical distances of Table 1. We thus propose that, on the basis of travel times, waveforms, and signal polarities, the emergent first arrivals seen at Parkfield are best explained in terms of fault zone head waves. If so, then other types of refracted head waves are also likely to occur. Examples are shear-mode head waves and mode-converted P to S and S to P refractions.

The fault zone head waves are confined to small regions in the vicinity of material interfaces such as the San Andreas fault and are therefore seemingly of local interest only. However, it is precisely the data from these regions that contain the details of earthquake processes and fault zone structure. Fault zone head waves can be mistakenly attributed to various source and medium effects. For example, a head wave propagating along the material interface with P wave velocity and then continuing into the faster medium as an S wave can have a short lag time after the initial P arrival, resulting in a complicated initial waveform. Such waveforms may lead to an assumption of a complex source behavior (for instance, a multiple-slip event). The complexity of the initial P waveforms in the earthquakes we examined increases from the northern station ST to the southern station FR (see, for example, Fig. 4). This increase in complexity may result in part from converted head waves separating in time from the direct P arrival as the source-receiver distance increases. As another example, a head wave that started as a P wave, converted to an S wave, and then continued to an observation point might have a predominantly SV motion, whereas the direct S wave may be characterized (for a strike-slip event) by a predominantly SH motion. The different travel times and motion polarities may be taken as evidence for shear wave splitting arising from anisotropy.

Our study indicates that fault zone head waves are common in the Parkfield seismograms recorded on the slower side of the fault. Fault zone head waves may have both negative and positive effects. On the negative side, misidentification of these phases as direct arrivals introduces errors in event location, earthquake mechanism, and other rupture process and medium property studies. On the positive side, proper analysis of fault zone head waves can be used to study material contrast across important structures such as the San Andreas fault. Careful monitoring of these phases may provide information on variation of fault zone material properties in time and space.

REFERENCES AND NOTES

1. Y. Ben-Zion, *Geophys. J. Int.* **98**, 213 (1989).
2. ———, *ibid.* **101**, 507 (1990).
3. ———, thesis, University of Southern California, Los Angeles (1990).
4. P. E. Malin, S. N. Blakeslee, M. G. Alvarez, A. J. Martin, *Science* **244**, 557 (1989).
5. R. S. Carmichael, Ed., *Handbook of Physical Properties of Rocks* (CRC Press, Boca Raton, FL, 1982), vol. 2.
6. A. W. Walter and W. D. Mooney, *Bull. Seismol. Soc. Am.* **72**, 1567 (1982).
7. J. H. Lees and P. E. Malin, *J. Geophys. Res.* **95**, 21793 (1990).

8. This work was funded by National Science Foundation grant EAR-8904259 (Y.B.-Z.) and U.S. Geological Survey grant 14-08-0001-G1793 (P.M.).

7 November 1990; accepted 24 January 1991

Microtektites, Microkrystites, and Spinels from a Late Pliocene Asteroid Impact in the Southern Ocean

STANLEY V. MARGOLIS,* PHILIPPE CLAEYS, FRANK T. KYTE

The properties of glassy spherules found in sedimentary deposits of a late Pliocene asteroid impact into the southeast Pacific are similar to those of both microtektites and microkrystites. These spherules probably formed from molten silicate droplets that condensed from an impact-generated vapor cloud. The spherules contain inclusions of magnesioferrite spinels similar to those in spherules found at the Cretaceous-Tertiary boundary, indicating that both sets of spherules are impact debris formed under similar physical and chemical conditions.

STUDIES OF LATE PLIOCENE DEEP-SEA sediments (*1–3*) have shown that ~2.3 million years ago an asteroid ~0.5 km in diameter impacted the subantarctic South Pacific Ocean in the region ~1400 km due west of Cape Horn. Sediment deposits recording this impact are enriched in Ir and Au and contain relatively coarse-grained (1 to 5 mm) impact debris. Most of this debris is a vesicular impact melt, composed of asteroidal material and traces of seawater salt from the oceanic impact. A small amount of the debris is unmelted fragments of the impacting mesosiderite asteroid. These fragments have been named the Eltanin meteorite. The deposits indicate that the impact was into the ocean basin, without significant excavation of sea-floor materials or incorporation of marine sediments or oceanic basement into the impact melt (*2*). We describe

S. V. Margolis and P. Claeys, Department of Geology, University of California, Davis, CA 95616.
F. T. Kyte, Institute of Geophysics and Planetary Physics, University of California, Los Angeles, CA 90024.

*To whom correspondence should be addressed.